

Closely Compacted $\text{TiNb}_2\text{O}_7\text{-C}$ Assembly for Fast-Charging Battery Anodes

Weiwei Liu, Jing Liu, Menghua Zhu, Wenyu Wang, and Yongming Sun*

Cite This: *ACS Appl. Energy Mater.* 2021, 4, 12319–12325

Read Online

ACCESS |



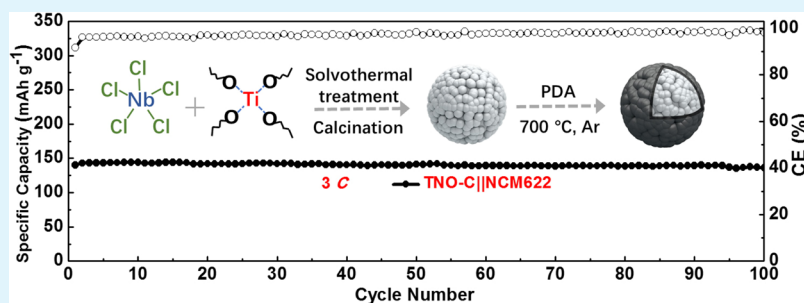
Metrics & More



Article Recommendations



Supporting Information



ABSTRACT: The fast-charging capability of lithium-ion batteries (LIBs) is becoming more important than before to meet the increasing requirements in practical applications. Because of safe working potential (above 1 V) and moderately high specific capacity, titanium niobium oxide (TiNb_2O_7 , TNO) shows great potential as a fast-charging anode. Herein, a TNO-C assembly consisting of active initial TNO nanoparticles with conformal carbon coating is fabricated. The small size of TNO nanoparticles provides a short diffusion distance for lithium ions, and surficial carbon layers enable good electronic conductivity within the entire assembly. Moreover, the compact structure within the TNO assembly and efficient space packing of spheroidal secondary particles are beneficial for close packing, leading to an overall short distance for electron transport and ion diffusion. As expected, the as-designed TNO-C electrode delivers a high capacity of 194 mAh g^{-1} under 10C, and 71% of capacity was achieved under 0.2C. Moreover, the TNO-C electrode shows stable cycling performance with capacity retention of 92.2% after 100 cycles under 2C. In addition, by pairing with a lithium nickel–cobalt manganese ($\text{LiNi}_{0.6}\text{Co}_{0.2}\text{Mn}_{0.2}\text{O}_2$, NCM) cathode, the full cell exhibits a high capacity of 140 mAh g^{-1} under 3C and a high capacity retention of 97.4% after 100 cycles. The rational design of a TNO-C assembly makes it an excellent anode candidate for fast-charging LIBs.

KEYWORDS: fast-charging anode, lithium-ion batteries, $\text{TiNb}_2\text{O}_7\text{-C}$, closely compacted, secondary particles

1. INTRODUCTION

Lithium-ion batteries (LIBs) are one of the most successful energy-storage technologies that are widely involved in portable electronic devices and electric vehicles.^{1–3} To meet the increasing demands of batteries in fast charging for various applications, anodes with high rate capability and good safety are being intensively pursued.^{4–6} Because of the sluggish lithium-intercalation kinetics and low lithiation potential (0.1 V vs Li/Li^+) of current graphite anodes, overpotential under high charging current densities can easily push the anode potential to the threshold for lithium-metal plating, leading to performance degradation and even safety concerns.^{7–9} $\text{Li}_4\text{Ti}_5\text{O}_{12}$ attracts abundant attention because of its safe lithiation potential of about 1.5 V versus Li^+/Li . However, its low theoretical specific capacity of 175 mAh g^{-1} significantly limits the energy density of batteries.^{10,11} Nb-based materials often possess fast ionic transport kinetics and show promise as anode materials with a high rate for high-power LIBs. For example, $\text{T-Nb}_2\text{O}_5$, $\text{Nb}_{18}\text{W}_{16}\text{O}_{93}$, and TiNb_2O_7 have been prepared and exhibited excellent rate capability as battery

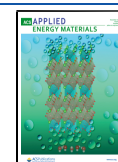
anode materials.^{6,12} Additionally, the inherent properties of bulk TiNb_2O_7 have been investigated from experimental and computational insights, and the results reveal its fundamental of the lithium-insertion mechanism.¹³ In these respects, titanium niobium oxide (TiNb_2O_7 , TNO) exhibits great advantages as a fast-charging anode material for LIBs because of its higher theoretical specific capacity (388 mAh g^{-1}) than $\text{Li}_4\text{Ti}_5\text{O}_{12}$, moderate lithiated potential of 1.5 V versus Li^+/Li on average, and a high ion-diffusion coefficient ($10^{-11} \text{ m}^2 \text{ s}^{-1}$).^{4,13–16}

In addition to the inherent properties of materials, a rational structure design of materials and electrodes with high ionic and

Received: July 20, 2021

Accepted: October 20, 2021

Published: November 1, 2021



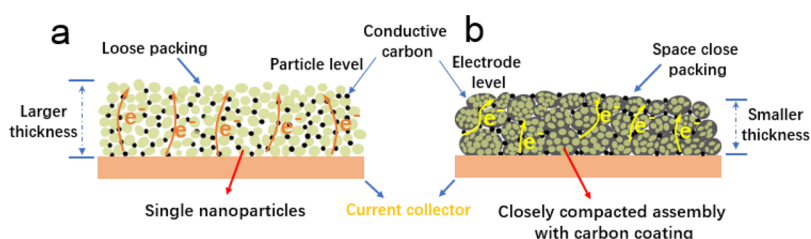


Figure 1. Schematic of electrodes with (a) nanoscale active materials and (b) micrometer-sized assembly of nanomaterials with carbon coating that increases the tap density and reduces the thickness of electrodes with the same areal capacity in comparison to single nanoparticles, which shortens the transfer pathways of charges and increases the volumetric capacity of electrodes and the energy density of batteries.



Figure 2. Synthesis schematic of the TNO-C materials.

electronic conductivity and reduced charge-transport distance can ensure rapid electrochemical reaction and endure good rate capability of anodes, and thus high power density of batteries.^{17,18} To enhance the ionic and electronic conductivity, the main strategies are decreasing the size of the active materials to the nanoscale to shorten the transport distance for ions at the particle level and compositing with conducting additives to improve the electric conductivity.^{19,20} However, small-sized nanomaterials will lead to a low tap density and thick electrode with the same mass loading, leading to a long electron and ion-transfer distance and eventually an inferior rate capability (Figure 1a).²¹ Additionally, the high surface area of active nanomaterials will cause severe side reactions with the electrolyte, resulting in degraded cycling. The increase in the electrode thickness and porosity also gives rise to an increase in the electrolyte adsorption of electrodes, limiting the volume energy density of LIBs.²² Closely compacted assembly of nanoparticles with a large size can tackle the issues that single nanoparticles bring in and realize a high volumetric capacity (Figure 1b).⁸ A further combination with conducting coating, such as the assembly of active materials, can help realize the high rate capability of practical battery anodes.

To realize a high-rate battery anode for fast-charging LIBs, herein, we reported closely compacted $\text{TiNb}_2\text{O}_7\text{-C}$ secondary particles consisting of TiNb_2O_7 nanoparticles with good electronic conductivity and fast charge-transport capability. As expected, the $\text{TiNb}_2\text{O}_7\text{-C}$ assembly exhibited high rate capability and showed 71% capacity at a high rate of 10C (calculated based on the value of 275 mAh g^{-1} at 0.2C). High cycling stability was realized at 2C, and the capacity retention was 92.2% after 100 cycles for half cells. A full cell of TNO-C||NCM was also fabricated and exhibited superior fast-charging ability at 3C, as well as high cycling stability. Such an assembly of TNO-C composites provides a successful example of the rational material structure design toward practical fast-charging LIB anodes.

2. EXPERIMENTAL SECTION

2.1. Synthesis of TiNb_2O_7 and $\text{TiNb}_2\text{O}_7\text{-C}$ Composites. The TNO nanospheres were prepared via a facile one-step solvothermal method.²³ In a typical procedure, 60 mL of ethyl alcohol was used to

dissolve 411 μL of tetrabutyl titanate ($\text{Ti}(\text{OC}_4\text{H}_9)_4$, Aladdin) and 648 mg of niobium chloride (NbCl_5 , Aladdin) under violent stirring until a uniform solution was formed. Subsequently, a homogeneous solution was transferred to an autoclave, which was treated at 210 $^\circ\text{C}$ for 21 h. White sediment was washed and collected after the solvothermal process by centrifugation. After drying at 70 $^\circ\text{C}$, the white powder was treated at 800 $^\circ\text{C}$ for 300 min in air with a heating rate of 2 $^\circ\text{C min}^{-1}$ to produce TNO material. To fabricate the TNO-C composite, 400 mg of TNO powder was dispersed in an aqueous solution containing 90 mg of dopamine. After stirring for 2.5 h, the solid product was collected by vacuum filtration and vacuum-dried at 60 $^\circ\text{C}$ overnight. The TNO-C material was obtained by the thermal annealing of the above-prepared solid product at 700 $^\circ\text{C}$ for 120 min under an argon atmosphere at a ramping rate of 2 $^\circ\text{C min}^{-1}$.

2.2. Material Characterization. The active materials involved were tested by field-emission scanning electron microscopy (FE-SEM, Nova NanoSEM 450), X-ray diffraction (XRD, x'pert3 powder) with a Cu radiation target, transmission electron microscopy (TEM, Tecnai G220), and Raman spectroscopy (LabRAM HR800). Thermogravimetric analysis (TGA, Diamond TG/DTA) was employed to investigate the ingredient weight ratio.

2.3. Electrochemical Measurements. The TNO and TNO-C electrodes were prepared by blending the active material, carbon black, and polyacrylic acid with a weight ratio of 8:1:1 in deionized water to a homogeneous slurry, which was then coated on a copper current collector using a doctor blade coating approach, and the corresponding electrode was achieved after vacuum drying and mechanical rolling. The NCM electrodes were prepared using the same procedure with the TNO electrodes, except for the binder use of polyvinylidene fluoride. The electrochemical performances were investigated with CR2032-type coin cells, which were assembled in a glovebox full of Ar with O_2 and H_2O contents both less than 0.1 ppm. The separator was Celgard 2500 membranes. LiPF_6 (1.0 M) was dissolved in ethylene carbonate and diethylcarbonate with a volume ratio of 1:1 and 5 wt % fluoroethylene carbonate (FEC) as the additive. A Neware multichannel battery testing instrument was used to test the galvanostatic discharge/charge (GDC) of TNO||Li half cells with a potential range of 1–3 V vs Li/Li^+ at 25 $^\circ\text{C}$ (1C = 300 mA g^{-1}). The specific capacity of the TNO-C composites was obtained by calculating based on the total mass without subtracting carbon. A VMP3 multichannel potentiostat (Bio-Logic) was used to perform electrochemical impedance spectroscopy (EIS) and cyclic voltammetry (CV). The EIS tests were conducted under an open-circuit potential with an amplitude of 10 mV at a frequency range from 100 kHz to 0.01 Hz. The electrochemical stability of NCM||TNO-C full cells was measured by galvanostatic and voltage charge/discharge on the Neware battery instrument within the voltage range from 1.5 to

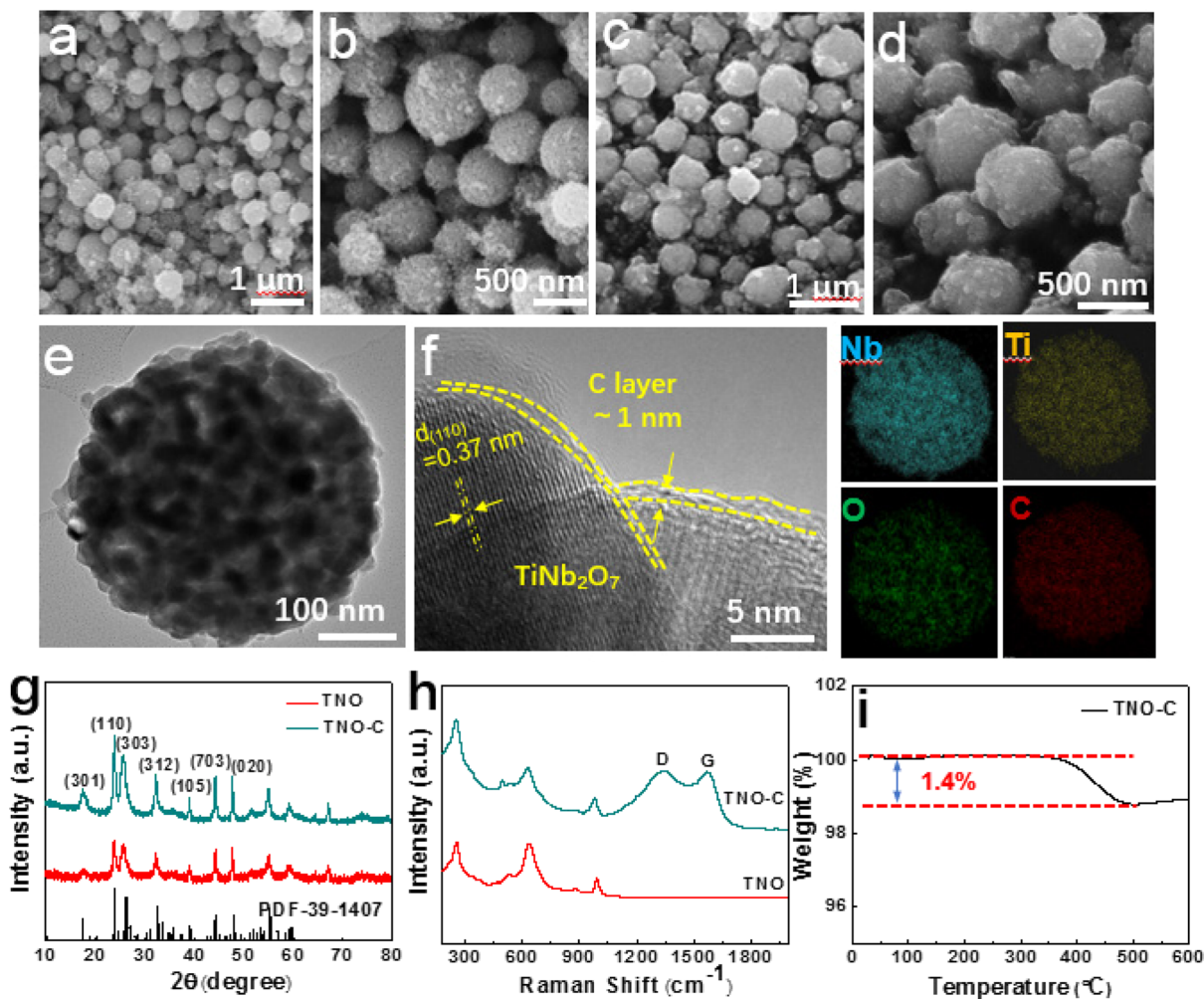


Figure 3. (a, b) SEM of TNO secondary particles. (c, d) SEM characterization of the TNO-C composite. (e) TEM and (f) HRTEM images for TNO-C, and the elemental mapping images of Nb, Ti, C, and O. (g) XRD and (h) Raman measurements for bare TNO and TNO-C composites. (i) TGA test for the TNO-C material.

2.8 V. The specific capacity of full cells was obtained by calculating based on the active mass loading of the NCM cathode, and the rate capability was evaluated based on the practical cathode capacity of 150 mA g^{-1} .

3. RESULTS AND DISCUSSION

The synthesis schematic of the TNO-C composite is shown in Figure 2, involving a solvothermal process and a subsequent carbonization operation. Shortly, secondary TNO particles are obtained in the solvothermal process under certain pressure and attraction force of different polarity charges. Subsequently, polydopamine is coated on the surface of the TNO particles using a solution approach, followed by carbonization under an Ar atmosphere to acquire the TNO-C composites.

The TNO intermediates from the solvothermal process and the bare TNO products after thermal annealing in air are characterized by SEM (Figure 3a,b). The secondary TNO particles show a spherical morphology with the size range between 400 and 800 nm. These secondary particles are densely compacted without showing pores on the surface but only a rough surface of the entire secondary assembly under SEM. As shown in Figure 3c, the spherical shape and submicroscale size of the secondary particles are well maintained for the TNO-C composite during the surface

polymerization of polydopamine and the calcination process. The surface of the TNO-C becomes smoother after carbon coating in comparison to the bare TNO (Figure 3d). The TEM results showed that the assembly of TNO-C spheres comprises closely compacted nanocrystals with diameters between 30 and 50 nm (Figure 3e). In addition, a uniform carbon nanolayer of ~ 1 nm covers the entire surface of the particles to improve the electric conductivity and protect the structural integrity of the TNO-C assembly during the charging/discharging process (Figure 3f). Moreover, lattice fringes with about 0.34 nm spacing are clearly observed, corresponding to the (003) lattice plane of TNO. The corresponding EDS mapping verifies the uniform distribution of Nb, Ti, O, and C elements in the TNO-C assemblies, demonstrating the successful fabrication of high-quality TNO-C composites.

XRD characterization is conducted to analyze the crystallinity and phase information of the prepared materials. As shown in Figure 3g, the XRD results for the TNO and TNO-C materials are nearly overlapped, and the main sharp diffraction peaks at 2θ values of 17.4 , 23.9 , 25.9 , 32.5 , and 47.8° correspond to the (301), (110), (303), (312), and (020) planes of TiNb_2O_7 (JCPDS no. 39-1407), suggesting the successful formation of the TNO phase. XRD measurement is

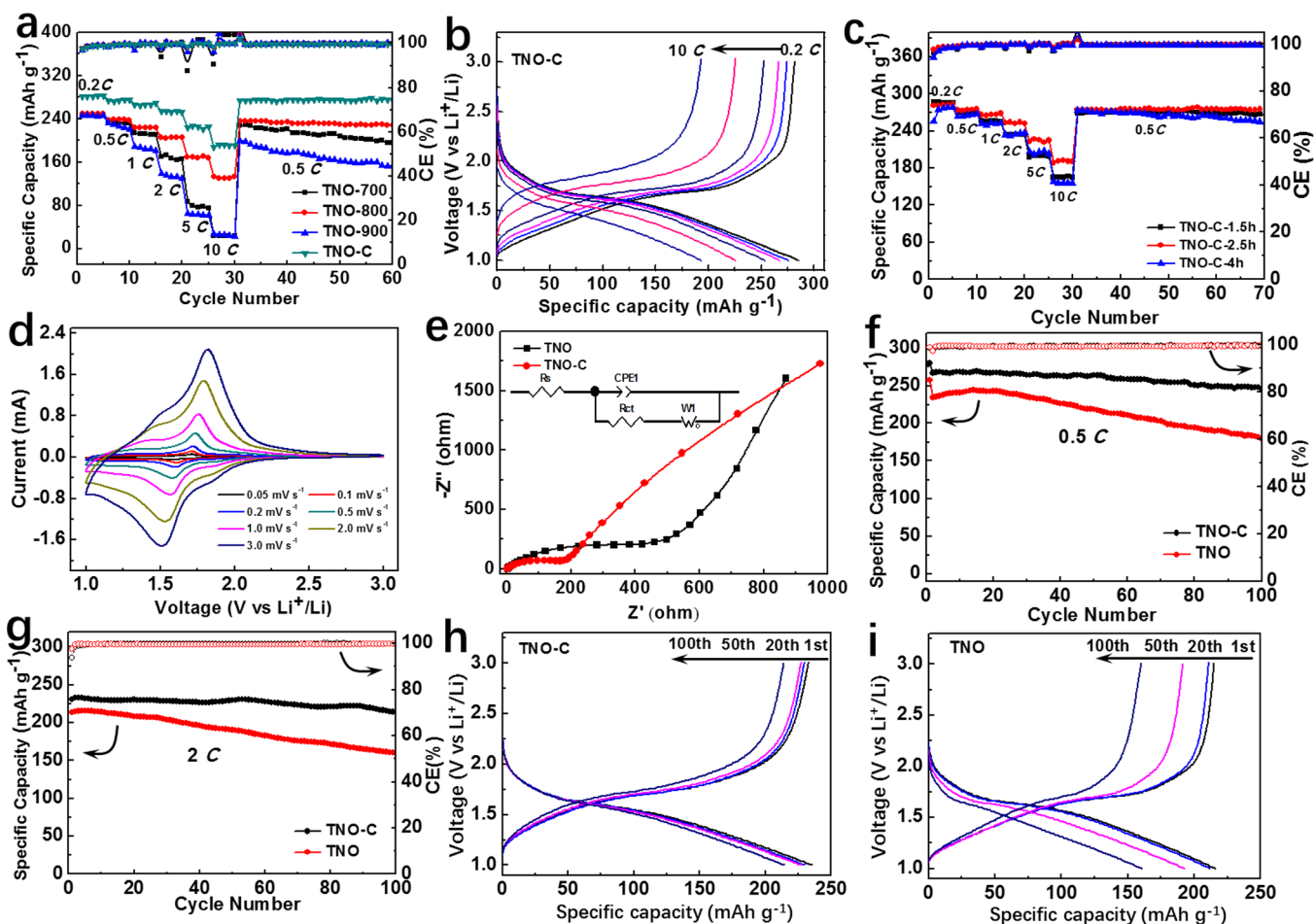


Figure 4. (a) Rate performance of the TNO-C composite and bare TNO fabricated using different calcination temperatures. (b) GDC curves of the TNO-C composite at a series of current densities. (c) Rate capability of TNO-C composites with different carbon contents by adjusting the polymerization time. (d) CV tests of the TNO-C composite. (e) Nyquist plots of the TNO and TNO-C composites before cycling. (f) Cycling performance comparison of the TNO-C composite and bare TNO at 0.5C and (g) 2C in half cells. (h) Corresponding GDC plots of the TNO-C composite and (i) bare TNO from different cycles at 2C.

also carried out for bare TNO materials achieved under other calcination temperatures (Figure S1). Their XRD patterns are nearly the same, except for the stronger crystallinity at a higher temperature of 900 °C. Raman spectroscopy was also performed to analyze the microstructures of bare TNO and TNO-C materials within the range of 200–2000 cm^{-1} (Figure 3h and Figure S2). The obvious band centered at 643 cm^{-1} results from the vibration of TiO_6 octahedra.²⁴ The two peaks located at 886 and 1003 cm^{-1} correspond to the phonon vibration of the TNO nanospheres, which are ascribed from the corner and edge-shared NbO_6 octahedra, respectively.²⁵ Two additional broad bands of the TNO-C composite located at 1340 and 1574 cm^{-1} correspond to the D and G peaks of the carbon layer.²⁶ The results of these above characterizations clearly evidence the successful fabrication of TNO-C assemblies.²⁷ TGA tests are conducted under ambient air at a heating rate of 5 °C min^{-1} to identify the carbon content ratio of TNO-C composites. For the oxidation of carbon, the total weight decreases with the temperature increasing to nearly 400 °C (Figure 3i). The lost mass percentage of carbon in the TNO-C is nearly 1.4%, according to the TGA report.

The impact of calcination temperature of bare TNO on the rate capability is first investigated. A series of bare TNO samples is synthesized using different calcination temperatures

from 700 to 900 °C (denoted as TNO-700, TNO-800, and TNO-900), and their rate capability is evaluated. The TNO-800 delivers high capacities of 248 mAh g^{-1} at 0.2C and 172 mAh g^{-1} at 5C with a capacity retention of 70%.^{28,29} The TNO-700 and TNO-900 exhibit similar capacities to the TNO-800 at 0.2C and 0.5C, respectively (Figure 4a). However, when the current density further increases, the reversible capacity dramatically decreases. For example, TNO-700 and TNO-900 deliver 79 and 63 mAh g^{-1} at a current density of 5C, respectively. The worse rate capability of TNO-700 and TNO-900 may result from the inferior ionic conductivity because of the low crystallinity (for TNO-700) or large initial particle size (for TNO-900). To further improve the rate capability of TNO-800, an ultrathin carbon nanolayer is conformally coated, which enhances the electronic conductivity. In comparison to TNO-800, the TNO-C composite exhibits 275 mAh g^{-1} at 0.2C and 194 mAh g^{-1} at 10C, with a capacity retention of 71%, which are among the best in the literature.^{27,29,30} When the rate returns to 0.5C, the capacity of the TNO-C composite recovers the initial value at 0.5C, and stable capacity-cycle number plots are also obtained, indicating the enhanced conductivity and structural stability due to the conformal ultrathin carbon coating.

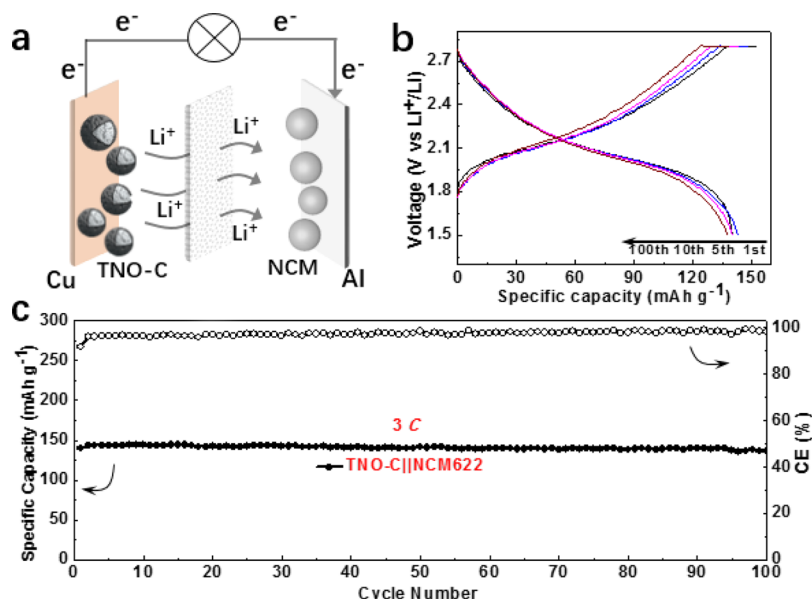


Figure 5. (a) TNO-C//NCM full cell schematic. (b) GDC plots at different cycles and (c) full cell cycling performance of TNO-C//NCM at 3C.

Figure 4b displays the GDC curves of the TNO-C (referred to TNO-C-2.5 h if stated otherwise) electrode at different current densities. A voltage plateau with an average voltage of ~ 1.6 V is observed, which is associated with the Li^+ -insertion behavior, and sloping regions (>1.65 and <1.55 V) are presented on the GDC curves, which correspond to the Li^+ extraction process.³⁰ As the current density increases from 0.2 to 5C, a little change in the average potential is observed, and the variation in electrochemical polarization is as small as 0.05 V, indicating the excellent charge-transfer capability of TNO-C.²¹ TNO-C materials with different mass contents of carbon are synthesized by adjusting the polymerization time of dopamine, and the corresponding samples are denoted as TNO-C-1.5 h, TNO-C-2.5 h, and TNO-C-4 h. As shown in Figure 4c, TNO-C-2.5 h demonstrates the best performance in terms of stability and capacity, demonstrating its optimized carbon coating.³¹

Figure 4d exhibits the CV tests of the TNO-C composite at scan rates from 0.05 to 3.0 mV s^{-1} and a pair of redox peaks are exhibited for all the CV curves. Only slight potential shifts of 0.08 and 0.1 mV are observed for the cathodic scan and anodic scan when the scan rate increases from 0.05 to 3 mV s^{-1} , indicating fast electrochemical reaction kinetics for the TNO-C composite.³² The EIS measurements are tested within the frequency range from 100 kHz to 0.01 Hz at the open-circuit voltage for the bare TNO and TNO-C to examine the electrochemical behavior (Figure 4e). The Nyquist curves show a semicircle at high frequencies, which is ascribed from the charge-transfer resistance (R_{ct}) and a slope at low frequencies, which represents for the ion-diffusion behavior inside the electrode.^{23,33} R_{ct} and the series resistance (R_s) value, which comprised the contact resistance at the interface of the electrolyte and electrode, internal resistance, and electrolyte resistance, are calculated with an equivalent circuit.³⁴ The R_s of the TNO-C composite and bare TNO are 1.55 and 1.88 Ω , respectively. The R_{ct} for TNO-C is calculated as 173.3 Ω , which is much smaller than that of the TNO-electrode (443.4 Ω). These results indicate that the thin carbon layer of the TNO-C nanospheres helps decrease the charge-transfer resistance, accounting for the improved rate

performance of the TNO-C composite. The calculated values of the lithium-ion diffusion coefficient before the cycling process are $4.2 \times 10^{-14} \text{ cm}^2 \text{ s}^{-1}$ for TNO-C and $4.8 \times 10^{-14} \text{ cm}^2 \text{ s}^{-1}$ for TNO, respectively, according to the EIS data. Similar values of the lithium-ion diffusion coefficient indicate that the carbon coating does not bring much negligible impact on the diffusion of the lithium ions. EIS confirms that the carbon content for the TNO-C composite can effectively increase the electrode electric conductivity, leading to improved electrochemical performance.

The cycling comparison between the TNO-C composite and bare TNO is first conducted at 0.5C within 1–3 V versus Li^+/Li , as shown in Figure 4f. High capacity retention of 93.1% is achieved for the TNO-C composite after 100 cycles in sharp contrast to 77% for the bare TNO. The cycling stability of the TNO-C composite is also evaluated at 2C (Figure 4g). After activation for five cycles at a low rate, the TNO-C composite displays 231 mAh g^{-1} at the first cycle at 2C and 213 mAh g^{-1} for the 100th cycle with a high capacity retention of 92.2%. In comparison, the bare TNO delivers a low capacity of 214 mAh g^{-1} at 2C and decays to 159 mAh g^{-1} after the 100th cycle with a low retention of 74.2%. The improved cycling stability at different C rates correlates with the fast charge-transfer capability and the structural integrity of the TNO-C composite. To deeply understand the electrochemical behavior, the corresponding voltage curves of bare TNO and the TNO-C composite at different cycles are shown in Figure 4h,i, which clearly illustrates the disparity in overpotential evolution. For the TNO-C composite, the GDC plots from the first cycle to the 100th cycle show the same shape with constant voltage plateau positions with only a slight increase in overpotential. In comparison, the bare TNO shows an obvious increase in overpotential after 20 cycles, indicating the inferior electrochemical stability.

Full cells fabricated with the NCM622 cathode and the TNO-C composite anode are also assembled to further evaluate the fast-charging capability of the TNO-C material (Figure 5a). Figure 5b shows the charge/discharge voltage profiles at different cycles of the TNO-C//NCM full cell at a fast-charging current of 3C. The charging capacity at 3C is

152.8 mAh g⁻¹, and the discharge capacity at 0.5C is 140.1 mAh g⁻¹, leading to a high Coulombic efficiency of 92%. Additionally, the voltage profiles at different cycles nearly overlap, which indicates the highly reversible intercalation/deintercalation mechanism of Li⁺. Figure 5c displays the cycle stability of the TNO-C||NCM full cell at 3C within the voltage range from 1.5 to 2.8 V. The full cell displays a discharge capacity of 140.1 mAh g⁻¹ for the initial cycle and 136.4 mAh g⁻¹ after 100 cycles with high retention of 97.4%. The excellent fast-charging capability of the TNO-C composite with high stability makes it a promising candidate for LIBs in high rate applications.

4. CONCLUSIONS

In summary, TNO-C assemblies in the submicrometer size are synthesized using a solvothermal method with the combination of conformal conductive carbon coating. The design of the secondary TNO structure and ultrathin carbon layer enhances the charge transfer within the electrode. Meanwhile, the submicrometer size and spherical morphology of the TNO-C composite are beneficial for the close compact of active materials and thus short charge-transfer distance at the electrode level. Combining with the intrinsic advantage of the moderate working potential, the obtained TNO-C composite exhibits a high capacity of 194 mAh g⁻¹ at 10C with a capacity retention of 71% (based on the value at 0.2C) and high stability with a capacity retention of 92.2% at 2C for 100 cycles in a half cell. Furthermore, the full cell TNO-C||NCM shows excellent cycle performance at a high charging rate of 3C with retention of 97.4% for 100 cycles. The facile fabrication of such a TNO-C composite with excellent electrochemical performance under high-rate conditions makes it a potential high-rate anode candidate for LIBs.

■ ASSOCIATED CONTENT

Supporting Information

The Supporting Information is available free of charge at <https://pubs.acs.org/doi/10.1021/acsaem.1c02144>.

XRD patterns of TNO-based materials; Raman spectra for a series of TNO-based materials; GITT tests for TNO and TNO-C anodes. (PDF)

■ AUTHOR INFORMATION

Corresponding Author

Yongming Sun – Wuhan National Laboratory for Optoelectronics, Huazhong University of Science and Technology, Wuhan 430074, China; orcid.org/0000-0001-8528-525X; Email: yongmingsun@hust.edu.cn

Authors

Weiwei Liu – Wuhan National Laboratory for Optoelectronics, Huazhong University of Science and Technology, Wuhan 430074, China

Jing Liu – Wuhan National Laboratory for Optoelectronics, Huazhong University of Science and Technology, Wuhan 430074, China

Menghua Zhu – Wuhan National Laboratory for Optoelectronics, Huazhong University of Science and Technology, Wuhan 430074, China; School of Materials Science and Engineering, Northwestern Polytechnical University, Xi'an 710072, China

Wenyu Wang – Wuhan National Laboratory for Optoelectronics, Huazhong University of Science and Technology, Wuhan 430074, China

Complete contact information is available at: <https://pubs.acs.org/doi/10.1021/acsaem.1c02144>

Notes

The authors declare no competing financial interest.

■ ACKNOWLEDGMENTS

This work is financially supported by the Innovation Fund of Wuhan National Laboratory for the Optoelectronics of Huazhong University of Science and Technology, Post-doctoral Innovative Research Post in Hubei Province (0106187142), and the Fundamental Research Funds for the Central University (3102020QD0408). We also thank the Analytical and Testing Center of the Huazhong University of Science and Technology as well as the Center for Nanoscale Characterization & Devices of the Wuhan National Laboratory for Optoelectronics for the characterization.

■ REFERENCES

- (1) Guo, B.; Yu, X.; Sun, X. G.; Chi, M.; Qiao, Z. A.; Liu, J.; Hu, Y. S.; Yang, X. Q.; Goodenough, J. B.; Dai, S. A long-life lithium-ion battery with a highly porous TiNb₂O₇ anode for large-scale electrical energy storage. *Energy Environ. Sci.* **2014**, *7*, 2220–2226.
- (2) Yu, Z.; Wang, H.; Kong, X.; Huang, W.; Tsao, Y.; Mackanic, D. G.; Wang, K.; Wang, X.; Huang, W.; Choudhury, S.; Zheng, Y.; Amanchukwu, C. V.; Hung, S. T.; Ma, Y.; Lomeli, E. G.; Qin, J.; Cui, Y.; Bao, Z. Molecular design for electrolyte solvents enabling energy-dense and long-cycling lithium metal batteries. *Nat. Energy* **2020**, *5*, 526–533.
- (3) Chen, T.; Jin, Y.; Lv, H.; Yang, A.; Liu, M.; Chen, B.; Xie, Y.; Chen, Q. Applications of lithium-ion batteries in grid-scale energy storage systems. *Trans. Tianjin Univ.* **2020**, *26*, 208–217.
- (4) Yuan, T.; Soule, L.; Zhao, B.; Zou, J.; Yang, J.; Liu, M.; Zheng, S. Recent advances in titanium niobium oxide anodes for high-power lithium-ion batteries. *Energy Fuels* **2020**, *34*, 13321–13334.
- (5) Lyu, H.; Li, J.; Wang, T.; Thapaliya, B. P.; Men, S.; Jafra, C. J.; Tao, R.; Sun, X.-G.; Dai, S. Carbon coated porous titanium niobium oxides as anode materials of lithium-ion batteries for extreme fast charge applications. *ACS Appl. Energy Mater* **2020**, *3*, 5657–5665.
- (6) Griffith, K. J.; Wiaderek, K. M.; Cibin, G.; Marbella, L. E.; Grey, C. P. Niobium tungsten oxides for high-rate lithium-ion energy storage. *Nature* **2018**, *559*, 556–563.
- (7) Park, H.; Wu, H. B.; Song, T.; David Lou, X. W.; Paik, U. Porosity-controlled TiNb₂O₇ microspheres with partial nitridation as a practical negative electrode for high-power lithium-ion batteries. *Adv. Energy Mater.* **2015**, *5*, No. 1401945.
- (8) Sun, Y.; Wang, L.; Li, Y.; Li, Y.; Lee, H. R.; Pei, A.; He, X.; Cui, Y. Design of red phosphorus nanostructured electrode for fast-charging lithium-ion batteries with high energy density. *Joule* **2019**, *3*, 1080–1093.
- (9) Wang, H.; Zhu, Y.; Kim, S. C.; Pei, A.; Li, Y.; Boyle, D. T.; Wang, H.; Zhang, Z.; Ye, Y.; Huang, W.; Liu, Y.; Xu, J.; Li, J.; Liu, F.; Cui, Y. Underpotential lithium plating on graphite anodes caused by temperature heterogeneity. *Proc. Natl. Acad. Sci. U. S. A.* **2020**, *117*, 29453–29461.
- (10) Babu, B.; Shaijumon, M. M. Studies on kinetics and diffusion characteristics of lithium ions in TiNb₂O₇. *Electrochim. Acta* **2020**, *345*, No. 136208.
- (11) Li, H.; Zhang, Y.; Tang, Y.; Zhao, F.; Zhao, B.; Hu, Y.; Murat, H.; Gao, S.; Liu, L. TiNb₂O₇ nanowires with high electrochemical performances as anodes for lithium ion batteries. *Appl. Surf. Sci.* **2019**, *475*, 942–946.

- (12) Lou, S.; Cheng, X.; Wang, L.; Gao, J.; Li, Q.; Ma, Y.; Gao, Y.; Zuo, P.; du, C.; Yin, G. High-rate capability of three-dimensionally ordered macroporous TiNb_2O_7 through Li^+ intercalation pseudocapacitance. *J. Power Sources* **2017**, *361*, 80–86.
- (13) Griffith, K. J.; Seymour, I. D.; Hope, M. A.; Butala, M. M.; Lamontagne, L. K.; Preefer, M. B.; Koçer, C. P.; Henkelman, G.; Morris, A. J.; Cliffe, M. J.; Dutton, S. E.; Grey, C. P. Ionic and Electronic Conduction in TiNb_2O_7 . *J. Am. Chem. Soc.* **2019**, *141*, 16706–16725.
- (14) Liu, G.; Zhao, L.; Sun, R.; Chen, W.; Hu, M.; Liu, M.; Duan, X.; Zhang, T. Mesoporous TiNb_2O_7 microspheres as high performance anode materials for lithium-ion batteries with high-rate capability and long cycle-life. *Electrochim. Acta* **2018**, *259*, 20–27.
- (15) Lou, S.; Cheng, X.; Gao, J.; Li, Q.; Wang, L.; Cao, Y.; Ma, Y.; Zuo, P.; Gao, Y.; du, C.; Huo, H.; Yin, G. Pseudocapacitive Li^+ intercalation in porous $\text{Ti}_2\text{Nb}_{10}\text{O}_{29}$ nanospheres enables ultra-fast lithium storage. *Energy Storage Mater.* **2018**, *11*, 57–66.
- (16) Lou, S.; Cheng, X.; Zhao, Y.; Lushington, A.; Gao, J.; Li, Q.; Zuo, P.; Wang, B.; Gao, Y.; Ma, Y.; du, C.; Yin, G.; Sun, X. Superior performance of ordered macroporous TiNb_2O_7 anodes for lithium ion batteries: Understanding from the structural and pseudocapacitive insights on achieving high rate capability. *Nano Energy* **2017**, *34*, 15–25.
- (17) Tu, S.; Chen, X.; Zhao, X.; Cheng, M.; Xiong, P.; He, Y.; Zhang, Q.; Xu, Y. A polysulfide-immobilizing polymer retards the shuttling of polysulfide intermediates in lithium-sulfur batteries. *Adv. Mater.* **2018**, *30*, No. 1804581.
- (18) Liu, W.; Zhu, M.; Liu, J.; Hu, W.; Li, X.; Liu, J. Synthesis of dense MoS_2 nanosheet layers on hollow carbon spheres and their applications in supercapacitors and the electrochemical hydrogen evolution reaction. *Inorg. Chem. Front.* **2018**, *5*, 2198–2204.
- (19) Jin, Y.; Zhu, B.; Lu, Z.; Liu, N.; Zhu, J. Challenges and recent progress in the development of Si anodes for lithium-ion battery. *Adv. Energy Mater.* **2017**, *7*, No. 1700715.
- (20) Lou, S.; Ma, Y.; Cheng, X.; Gao, J.; Gao, Y.; Zuo, P.; du, C.; Yin, G. Facile synthesis of nanostructured TiNb_2O_7 anode materials with superior performance for high-rate lithium ion batteries. *Chem. Commun.* **2015**, *51*, 17293–17296.
- (21) Xu, Q.; Li, J. Y.; Sun, J. K.; Yin, Y. X.; Wan, L. J.; Guo, Y. G. Watermelon-Inspired Si/C microspheres with hierarchical buffer structures for densely compacted lithium-ion battery anodes. *Adv. Energy Mater.* **2017**, *7*, No. 1601481.
- (22) Li, G.; Li, J. Y.; Yue, F. S.; Xu, Q.; Zuo, T. T.; Yin, Y. X.; Guo, Y. G. Reducing the volume deformation of high capacity $\text{SiO}_x/\text{G}/\text{C}$ anode toward industrial application in high energy density lithium-ion batteries. *Nano Energy* **2019**, *60*, 485–492.
- (23) Yao, M.; Liu, A.; Xing, C.; Li, B.; Pan, S.; Zhang, J.; Su, P.; Zhang, H. Asymmetric supercapacitor comprising a core-shell $\text{TiNb}_2\text{O}_7@/\text{MoS}_2/\text{C}$ anode and a high voltage ionogel electrolyte. *Chem. Eng. J.* **2020**, *394*, No. 124883.
- (24) Qian, R.; Yang, C.; Ma, D.; Li, K.; Feng, T.; Feng, J.; Pan, J. H. Robust lithium storage of block copolymer-templated mesoporous TiNb_2O_7 and $\text{TiNb}_2\text{O}_7@/\text{C}$ anodes evaluated in half-cell and full-battery configurations. *Electrochim. Acta* **2021**, *379*, No. 138179.
- (25) Ise, K.; Morimoto, S.; Harada, Y.; Takami, N. Large lithium storage in highly crystalline TiNb_2O_7 nanoparticles synthesized by a hydrothermal method as anodes for lithium-ion batteries. *Solid State Ionics* **2018**, *320*, 7–15.
- (26) Liu, W.; Liu, J.; Zhu, M.; Wang, W.; Wang, L.; Xie, S.; Wang, L.; Yang, X.; He, X.; Sun, Y. Recycling of lignin and Si waste for advanced Si/C battery anodes. *ACS Appl. Mater. Interfaces* **2020**, *12*, 57055–57063.
- (27) Pham-Cong, D.; Choi, J. H.; Yun, J.; Bandarenka, A. S.; Kim, J.; Braun, P. V.; Jeong, S. Y.; Cho, C. R. Synergistically enhanced electrochemical performance of hierarchical $\text{MoS}_2/\text{TiNb}_2\text{O}_7$ hetero-nanostructures as anode materials for Li-Ion batteries. *ACS Nano* **2017**, *11*, 1026–1033.
- (28) Fei, L.; Xu, Y.; Wu, X.; Li, Y.; Xie, P.; Deng, S.; Smirnov, S.; Luo, H. SBA-15 confined synthesis of TiNb_2O_7 nanoparticles for lithium-ion batteries. *Nanoscale* **2013**, *5*, 11102–11107.
- (29) Yang, C.; Lin, C.; Lin, S.; Chen, Y.; Li, J. $\text{Cu}_{0.02}\text{Ti}_{0.94}\text{Nb}_{2.04}\text{O}_7$: An advanced anode material for lithium-ion batteries of electric vehicles. *J. Power Sources* **2016**, *328*, 336–344.
- (30) Li, H.; Shen, L.; Pang, G.; Fang, S.; Luo, H.; Yang, K.; Zhang, X. TiNb_2O_7 nanoparticles assembled into hierarchical microspheres as high-rate capability and long-cycle-life anode materials for lithium ion batteries. *Nanoscale* **2015**, *7*, 619–624.
- (31) Tian, T.; Lu, L. L.; Yin, Y. C.; Li, F.; Zhang, T. W.; Song, Y. H.; Tan, Y. H.; Yao, H. B. Multiscale designed niobium titanium oxide anode for fast charging lithium ion batteries. *Adv. Funct. Mater.* **2021**, *31*, No. 2007419.
- (32) Zhu, G.; Li, Q.; Zhao, Y.; Che, R. Nanoporous $\text{TiNb}_2\text{O}_7/\text{C}$ composite microspheres with three-dimensional conductive network for long-cycle-life and high-rate-capability anode materials for lithium-ion batteries. *ACS Appl. Mater. Interfaces* **2017**, *9*, 41258–41264.
- (33) Yin, L.; Pham-Cong, D.; Jeon, I.; Kim, J. P.; Cho, J.; Jeong, S. Y.; Woo Lee, H.; Cho, C. R. Electrochemical performance of vertically grown WS_2 layers on TiNb_2O_7 nanostructures for lithium-ion battery anodes. *Chem. Eng. J.* **2020**, *382*, No. 122800.
- (34) Liu, W.; Zhu, M.; Liu, J.; Li, X.; Liu, J. Flexible asymmetric supercapacitor with high energy density based on optimized MnO_2 cathode and Fe_2O_3 anode. *Chin. Chem. Lett.* **2019**, *30*, 750–756.